

## Superstructuring in the bornite–digenite series: a high-resolution electron microscopy study

LARRY PIERCE

*Department of Chemistry, Arizona State University  
Tempe, Arizona 85281*

AND PETER R. BUSECK

*Departments of Geology and Chemistry  
Arizona State University, Tempe, Arizona 85281*

### Abstract

Bornite and digenite were studied by electron microscope high-resolution imaging and selected-area diffraction. Dark-field as well as bright-field imaging were found to be well-suited to the study of sulfide superstructures, especially when the subcell structure is known and can be recognized in images. The dark-field mode provides images with more detail and greater resolution than the more usual bright-field mode, resulting in clear representations of superstructures and details down to 1.9Å. Thermal and compositional changes induced by electron bombardment in the microscope resulted in the formation of the entire reported range of superstructures ( $2a$  to  $6a$ ) along the bornite–digenite join, and the observation of many transformations between superstructures.

An essential part of superstructuring in the series appears to be a separation into vacancy-rich and vacancy-poor clusters. This separation gives rise to periodic compositional modulations and positional displacements in the structures. Also, in images of the  $6a$  member of the series, we see structural dissimilarities between clusters and structural discontinuities due to mismatch of lattice spacings. These features imply that members in the bornite–digenite series result from arrested exsolution.

For any given supercell size, a number of polymorphic types exist, distinguished by their diffraction patterns. Transformations between structural types are seen, in many cases, to be continuous. The features in the diffraction patterns of bornite–digenite structures are apparently produced by a combination of (1) vacancy clustering, (2) various ordered or semi-ordered arrangements of vacancies, and (3) distortion resulting from (1) and (2).

### Introduction

Bornite,  $\text{Cu}_5\text{FeS}_4$ , and digenite,  $\text{Cu}_9\text{S}_5$ , occur in many ores and are of great economic importance. Their crystallography is also of interest; structure determination by conventional means is complicated by the occurrence of many superstructures, defect structures, disorder, sluggish reaction kinetics, and metastability. Despite extensive study, the structures of bornite, digenite, and the compounds intermediate in composition are not satisfactorily known.

The extensive literature on the size of superstructures, compositions and approximate stability ranges of members of the bornite–digenite (bn–dg) series is summarized in Figure 1. Variations in metal:sulfur and copper:iron ratios are accom-

modated by up to 25 percent vacancies in the metal sites. Ordering of these vacancies produces a series of superstructures whose cells range in size from twice ( $2a$ , where  $a = \sim 5.5\text{Å}$ ), to six times ( $6a$ ) the subcell dimension. There is also a superstructure displaying non-integral diffraction spacings ( $Na$ ,  $4 \leq N \leq 6$ ). The reason for the many superstructures is unknown.

A problem of long-standing crystallographic interest is the origin of certain non-systematic extinctions in the diffraction patterns of some superstructures in the bn–dg series. In these patterns, superstructure reflections only occur along the  $(111)_{\text{subcell}}$  directions of the reciprocal lattice (Fig. 2). An explanation was first provided by Donnay *et al.* (1958), who proposed a rhombohedral unit cell for digenite ( $5a$ ) which,

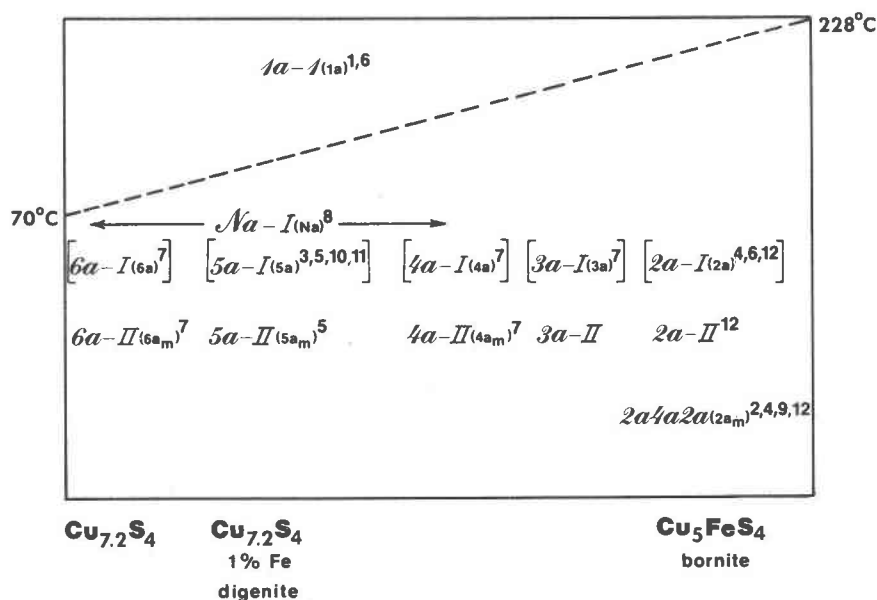


Fig. 1. The approximate composition and temperature ranges for reported bn-dg superstructures. Structures are listed according to the nomenclature in the present paper. The nomenclature following the conventions proposed by Morimoto and co-workers is given in parentheses. Phases reported as metastable are in brackets. An additional digenite-like superstructure which is not in this binary system is anilite ( $\text{Cu}_7\text{S}_4$ ,  $a=b=\sqrt{2}a$ ,  $c=a$ ; Koto and Morimoto, 1970). Superscripts denote references: (1) Tune' and Adams (1949); (2) Frueh (1950); (3) Donnay *et al.* (1958); (4) Morimoto and Kullerud (1961); (5) Morimoto and Kullerud (1963); (6) Morimoto (1964); (7) Morimoto and Kullerud (1966); (8) Morimoto and Gyobu (1971); (9) Koto and Morimoto (1975); (10) Manolikas *et al.* (1976); (11) Putnis (1977); (12) Putnis and Grace (1976).

when multiply twinned, appears to have cubic symmetry. This hypothesis was extended to the  $2a$  structure by Morimoto (1964), and to the remainder of the bn-dg series by Morimoto and Kullerud (1966). However, the kind of twinning which would explain the extinctions was not found in electron microscopic investigations of bornite and digenite by either Pierce and Buseck (1975), Manolikas *et al.* (1976), or Putnis (1977), and consequently a new or modified model is necessary.

Our previous experience with pyrrhotite (Pierce and Buseck, 1974, 1976) showed that high-resolution transmission electron microscopy is an extremely useful method of elucidating complicated structures of sulfides. High-resolution electron imaging enables the study of structural details averaged over as few as  $\sim 5$  unit cells and can provide data for projected areas smaller than one unit cell. Thus electron microscopy is useful in the study of minerals in which intimate twinning is suspected, such as the bn-dg series. Furthermore, electron diffraction patterns and images are seen immediately using a fluorescent screen, allowing the observation of phase transformations in progress. It therefore seemed logical to bring the power of this technique to bear on the complex problems of the bn-dg series.

### Nomenclature

The great number of superstructures seen in this study and the complexity of their inter-relationships require that the nomenclature be defined. The nomenclature adopted for this paper generally follows that of Morimoto and co-workers, but has been modified in order to be compatible with the discovery of the  $2a-II$  structure. Superstructures are named as multiples of the  $a$ -dimension of the cubic sub-cell (*e.g.*, low bornite =  $2a4a2a$ ). Isometric structures are abbreviated by listing only one dimension (*e.g.*,  $3a3a3a = 3a$ ).

In a number of cases, more than one structure type has the same unit-cell dimensions. For the series of isometric superstructures with dimensions  $2a$ ,  $3a$ ,  $4a$ ,  $5a$ , and  $6a$ , two different types having closely related diffraction patterns and electron images exist. Distinction between the two types is made by adding a Roman numeral to the dimensions of the unit cell. Thus, structures that have diffraction patterns with the non-systematic extinctions mentioned above are designated collectively as the *type I* structures or individually as  $2a-I$ ,  $3a-I$ ,  $4a-I$ , *etc.* The second type of structures has diffraction patterns with only systematic extinctions, and these structures are designated

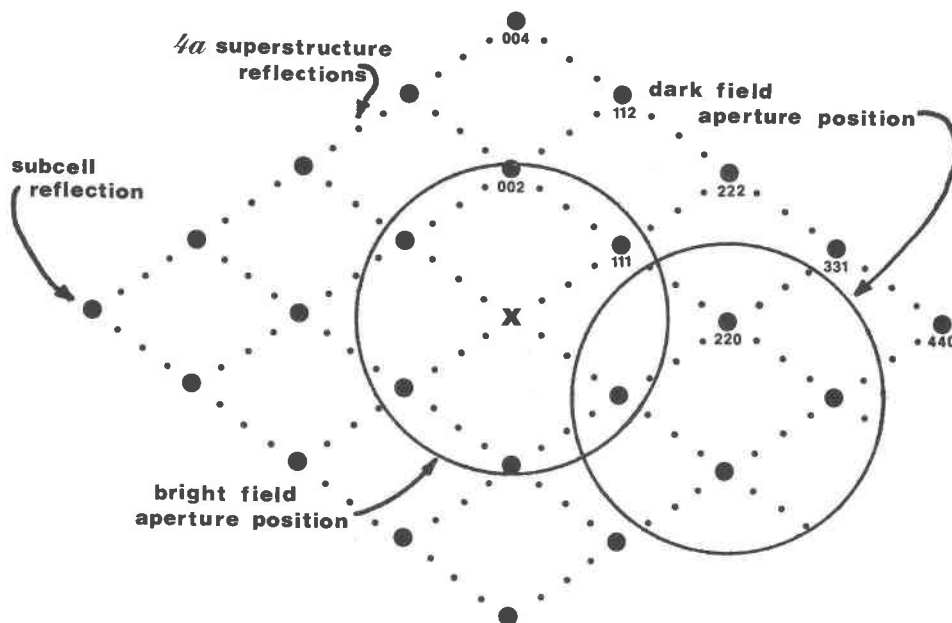


Fig. 2. A schematic diffraction pattern of the  $4a$ -I superstructure as viewed with the electron beam parallel to  $[1\bar{1}0]$ . The diamond-shaped areas in which superstructure reflections are extinct typify diffraction patterns of the *type I* structures. Beams falling within the bright-field aperture (indicated by circle) contribute to a bright-field image. In dark-field imaging, the incident beam is tilted so that the objective aperture allows only diffracted beams to contribute to the image. The beams contributing to dark-field images in the present paper are those within the circle marked "dark field aperture position."

the *type II* structures or  $2a$ -II,  $3a$ -II,  $4a$ -II, etc. The non-integral superstructure is called *Na-I* because of its similarity to the other *type I* structures, even though no corresponding *Na-II* structure has been reported as yet.

Other structures were found that were neither *type I* nor *II*. These are named by their cell size and an Arabic numeral (e.g.,  $1a$ -1,  $1a$ -2;  $1a1a2a$ -1,  $1a1a2a$ -2).

### Experimental

Samples of bornite from Superior, Ajo, and Bisbee, Arizona, and two samples of digenite containing minor bornite from Butte, Montana, were ground in acetone, suspended on holey grids as described in Buseck and Iijima (1974), and observed with a JEM 100B electron microscope at 100kV accelerating potential. Crystal fragments were observed at a direct magnification of about  $5,000,000\times$ . All images were photographed with  $(101)_{\text{subcell}}$  oriented parallel to the electron beam. This orientation was chosen, as it is a prominent zone which provides a clear view of superstructures along two  $(111)_{\text{subcell}}$  directions.

### Image interpretation

The interpretation of the intensity fluctuations in images from high-resolution bright-field electron mi-

croscopy (in which the undiffracted central beam is allowed to contribute to the images; Fig. 2) can be straightforward, as shown by both theory and experiment (e.g., Iijima, 1973; Buseck and Iijima, 1974; Cowley and Iijima, 1976). Images of structure are obtained for certain values of objective lens defocus and aperture size. Directly interpretable resolution under these conditions is limited to about  $3.5\text{\AA}$  for the JEM 100B microscope. The intensity in a bright-field image crudely resembles a two-dimensional projection of potential in the crystal. Projections of atoms or groups of atoms in the crystal appear dark in the image. Roughly speaking, the heavier the atoms or the greater the number of atoms in the projection, the darker the corresponding area in the image. The more vacancies in the projection, the lighter the corresponding area in the image.

For dark-field electron microscopy (in which only diffracted beams are allowed to contribute to the image; Fig. 2), conditions under which representative structure images are obtained are not as well known in either theory or practice. Theory indicates that dark-field microscopy might produce structure images having greater resolution and better contrast than bright-field, but with reversed contrast (Cowley, 1975). Our experience thus far supports these predictions,

and useful structure images of vacancy distributions of pyrrhotite have been obtained (Pierce and Buseck, 1974, 1976). Further, we have seen an encouraging correspondence between dark-field images, bright-field images, and computer-simulated bright-field images (generated by programs FCOEFF and DEFECT; Skarnulis, 1975) of known structures. In the present study, a relationship has been established between the known structure of low bornite (Koto and Morimoto, 1975) and the details of its dark-field images. Subsequently, an analogous interpretation can be applied to images from unknown but related structures.

In the case of the bn-dg series, dark-field imaging is especially useful for observing details of the subcell structure. Figure 2 shows that the only subcell reflections contributing to the bright-field image are those that are diffracted at relatively high angles. This means that, due to spherical and chromatic aberrations and beam divergence, these peripheral beams will not contribute to the image as strongly as those beams closer to the axis. Thus the bright-field image consists only of diffuse superstructure fringes, with almost no detail of the substructure. The use of the dark-field mode allows subcell reflections to be placed close to the objective lens axis while retaining a large number of superstructure reflections within the aperture. This results in an image with the same details of superstructure as the bright-field image (albeit with reversed contrast) except that it also provides detail on the subcell level. The most useful subcell detail consists of a pattern of dots 3.1 Å apart, and occurs at the value of defocus which produces the image of greatest contrast, thus facilitating proper defocussing. In this particular case, dark-field imaging produces greater resolution and is thus clearly superior to bright-field, and so is used extensively in this study.

Electron images are two-dimensional projections of three-dimensional structures. Thus our knowledge of structure perpendicular to the image plane is limited. However, for the bn-dg structures previously described as cubic and consistent with our observations, we may infer three-dimensional information by symmetry. For structures not previously described, we have assumed the smallest unit cell consistent with the projected image.

Care must be taken in the interpretation of features that appear to result from disorder, since an overlap of two ordered structures can produce similar features.

#### *Beam heating effects*

Electron-beam irradiation of bornite and digenite can produce both thermal and compositional changes

in the sample. Most electrons interacting with the crystal diffract and pass through without significant transfer of energy. However, those that undergo inelastic collisions impart considerable energy to atoms in the crystal. This results in a great enhancement of diffusion and ionization phenomena, which may produce compositional inhomogeneities in an unevenly irradiated crystal. Uneven irradiation is unavoidable for high-resolution imaging in larger (>200 Å diameter) crystals. Additionally, the absorbed energy is transferred throughout the entire crystal via lattice vibrations. This general increase in crystal energy is equivalent to a rise in apparent sample temperature, and can result in transformations to high-temperature polymorphs during beam irradiation. The apparent temperature of the crystal can be roughly controlled by varying the current in the condenser lens of the microscope. Thus, the many transformations in the bn-dg series can be promoted and studied as they occur.

The *3a-I* and *3a-II* structures occur in the microscope due to a compositional change. A small crystal of bornite (initially *2a4a2a*) was heated and cooled at various rates while carefully maintaining uniform beam intensity on the crystal, thus avoiding thermal gradients and the possible resulting diffusion. Superstructures of *3a* periodicity were not observed in these uniformly-heated crystals, contrary to the observations of Putnis and Grace (1976). The same crystal was then heated while purposely creating a thermal gradient with the electron beam. Subsequent cooling produced *3a* periodicities in the part of the crystal that had been the hottest. Since a *3a* periodicity is reported for a less iron-rich composition than that of bornite (Morimoto and Kullerud, 1966), apparently iron diffuses away from the heat of the beam.

Structures having *4a* periodicities were observed to form in two ways: (1) *4a-I* and *4a-II* were formed during a compositional change during uneven beam heating of bornite. This change is similar to but perhaps greater than that which produces the *3a* structures. (2) Low bornite was altered to *4a-II* during several days of storage of crushed samples under acetone. Whether oxidation or some other alteration caused the change is unknown. The diffraction pattern and image of the material produced in this manner, however, is the same as those of the structure produced in (1).

The *6a-I* and *6a-II* superstructures were described by Morimoto and Kullerud (1966) for synthetic  $\text{Cu}_9\text{S}_5$ . In the microscope, the *6a-I* structure can be produced from digenite (*5a-I*) starting material. Digenite is heated with the electron beam to trans-

form it to the  $1a-1$  structure. If cooled immediately, the  $5a-1$  structure returns. Continued heating in the  $1a-1$  stability field, however, produces a change, perhaps in composition, after which the  $6a-1$  structure appears upon cooling (see also Putnis, 1977).

### Structure models

We have formulated models based on images for some bn-dg superstructures. Their validity is determined by the extent to which their hypothetical X-ray diffraction patterns (calculated using the CRYSTALS system of programs; Rollett and Caruthers, personal communication, 1974) match the features of published X-ray and experimental electron diffraction patterns. Where intensity data are available ( $2a-1$ ; Morimoto, 1964), detailed comparison has been possible. Models formulated for the  $2a-1$  bornite and  $Na-1$  digenite structures will serve to illustrate the structural problems of the entire series, and will be discussed in the  $2a-1$  and  $Na-1$  sections.

### Discussion

Electron images and diffraction patterns have been obtained for a wide variety of superstructure types within the bn-dg series. They will be discussed approximately in order of increasing superstructure size, with a few miscellaneous superstructures at the end.

#### $1a-1$ , $1a-2$

The cubic subcell of structures in the bn-dg series is shown in Figure 3a. Above  $\sim 228^\circ\text{C}$  for bornite and  $\sim 70^\circ$  for digenite, the vacancies in the eight metal sites are disordered and the  $1a-1$  structure is stable (Morimoto and Kullerud, 1961, 1963). The diffraction pattern of  $1a-1$  is illustrated in Figure 4a, and a dark-field electron micrograph of the  $1a-1$  structure is shown in Figure 4b. The image consists of rows of white dots  $3.1\text{\AA}$  apart; this is an image of the subcell structure of the bn-dg series. A similar pattern occurs in other images of bn-dg superstructures.

Electron diffraction patterns of the  $1a-1$  structure of bornite show diffuse scattering between reflections along  $\langle 111 \rangle$  directions (also reported in Putnis and Grace, 1976), Figure 4c, as an intermediate state between the  $1a-1$  and  $2a-1$  structures for crystals of bornite composition. A similar occurrence of satellite reflections ( $1/5 \ 1/5 \ 1/5_{\text{subcell}}$ ) for digenite was reported by Putnis (1977). This appears to be the result of incipient vacancy clustering, as suggested by the irregular intensity fluctuations in the dark-field image in Figure 4d.

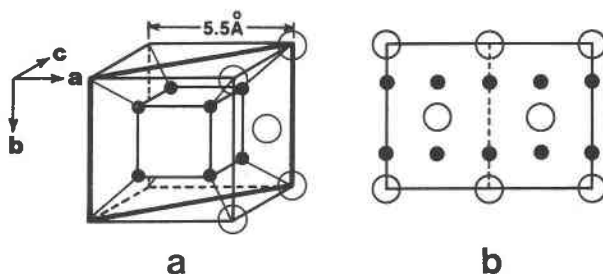


Fig. 3. The anti-fluorite type ( $a = 5.5\text{\AA}$ ) subcell of superstructures in the bn-dg series. (a) A perspective drawing. The unconventional orientation of the drawing (and all subsequent drawings in this paper) was chosen to approximate the view obtained in images. Sulfur atoms (open circles) are cubic-closest-packed and are located on a face-centered cubic lattice with  $a = \sim 5.5\text{\AA}$  (for simplicity, only one face of sulfur atoms is shown). Metal atoms (solid circles) are in the tetrahedral interstices of the sulfur framework and thus form an inner cube with  $a = \sim 2.75\text{\AA}$ . Heavy lines indicate the  $\langle 101 \rangle$  plane, onto which the structure is projected in (b). (b) A projection onto  $\langle 101 \rangle$ , the view of the structure presented by images in this paper.

Mention should be made of one image consisting of dim fringes  $1.9\text{\AA}$  by  $2.7\text{\AA}$  apart. This is a remarkably different image than that of  $1a-1$ , but could arise from a unit cell of the same size. The structure producing the image is here called  $1a-2$ , to indicate that more than one  $1a$  structure may exist.

#### Low bornite $2a4a2a$

The stable low-temperature phase of bornite composition has an orthorhombic superstructure  $2a4a2a$ ,  $Pbca$  (Koto and Morimoto, 1975). A portion of its diffraction pattern is illustrated in Figure 5a. The structure consists of a three-dimensional checkerboard alternation of subcells with filled metal sites and subcells with an ordered arrangement of four filled and four vacant sites (Fig. 5b). The vacancies within a subcell can be described as occurring at the vertices of a tetrahedron and, as such, can occur in two different orientations in the supercell, labeled  $A$  and  $B$  in Figure 5b. The segregation of vacancies into alternate subcells can be described as the formation of vacancy clusters of dimensions  $1a \times 1a \times 1a$ . The reason for such clustering was not given by Koto and Morimoto. Similar vacancy clustering, though, is central to the descriptions that follow of other superstructures in the bn-dg series.

Bright- and dark-field images of low bornite are shown in Figures 5c and 5d, respectively. The interpretations (schematic insets) of the images were derived by comparing computer-simulated bright-field images to actual bright- and dark-field photographs. The intensity fluctuations in the bright-field photo-

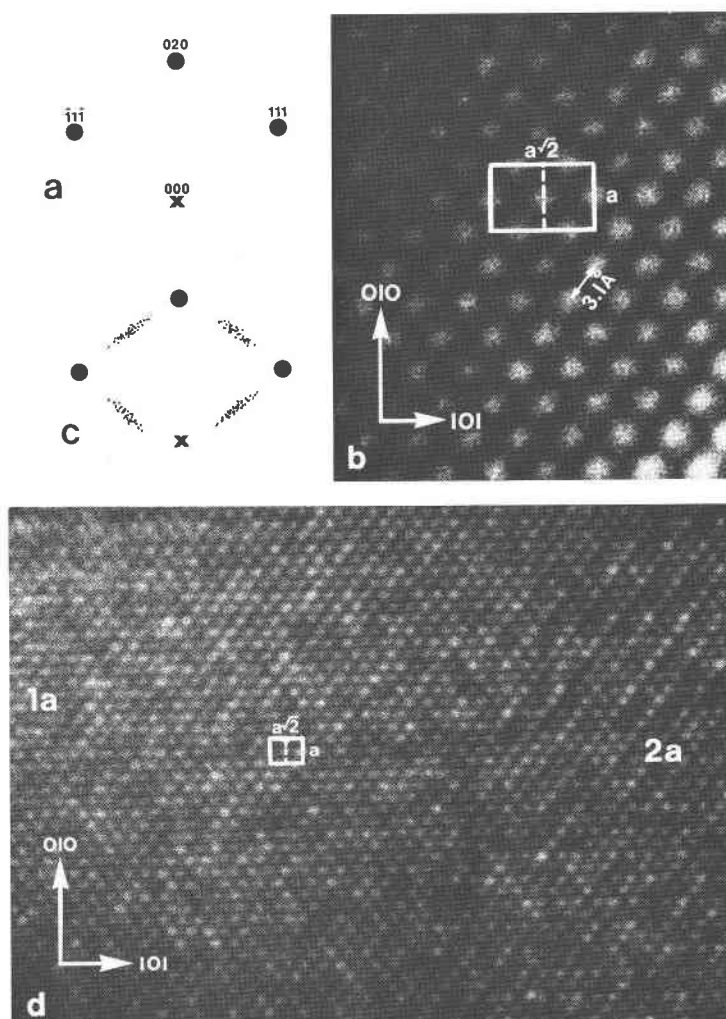


Fig. 4. The  $1a-1$  structure (Magma, Arizona, bornite starting material). (a) A portion of the diffraction pattern of  $1a-1$ . Subsequent illustrations of diffraction patterns will be of the same portion. (b) A dark-field image. A projected unit cell, similar to Fig. 3b, is illustrated. There is no superstructure, so all that is visible is a pattern of dots 3.1 Å apart, corresponding to details of the subcell structure. The dots bear a limited resemblance to the projected potential in the unit cell. Similar patterns will be present in dark-field images of many bn-dg superstructures. (c) A diffraction pattern of  $1a-1$  showing diffuse reflections indicative of crude superstructuring of approximately  $2a$  periodicity. (d) A dark-field image. The left side of the photograph contains dots of approximately equal intensities: an image of the normal  $1a-1$  structure. The middle of the photograph contains dots of varying intensities, probably a result of vacancy clustering, and perhaps producing the diffuse reflections in (c). At the extreme right, alternating bright and dim dots indicate a superstructure of  $2a$  periodicity beginning to form. Thus, from left to right in the photograph, a gradual transition from  $1a-1$  to  $2a$  superstructure can be observed.

graph are primarily due to the superstructure, for reasons explained above, and are directly related to vacancy concentrations. In the dark-field image the bright-field contrast is approximately reversed and subcell details are also present. These images can be directly related to the known structure of low bornite. For superstructures that are not well known, images can be interpreted by analogy to images of low bornite.

#### $2a-1$

Morimoto and Kullerud (1961) first reported the  $2a-1$  structure as a metastable polymorph of bornite, obtained by rapid cooling from the  $1a-1$  structure. A portion of the diffraction pattern of  $2a-1$ , showing  $002_{\text{super-cell}}$  extinct, is illustrated in Figure 6a. Morimoto (1964) found that this structure did not refine in its apparent space group,  $Fd3m$ , and he used a twin-

ning model to explain the extinctions and to refine the structure.

The  $2a-I$  structure, as identified by its electron diffraction pattern, can be produced from bornite in the microscope by varying the intensity of the electron beam (using different condenser-lens currents and apertures). The structures observed in bornite composition crystals are (in order of appearance with decreasing temperature)  $1a-I$ ,  $2a-I$ ,  $2a-II$ , low bornite. Transformations between them were found to be reversible and continuous over a range of temper-

atures. The  $1a-I$  structure was not quenchable. Images of the  $2a-I$  structure appear identical to images of low bornite (although the structures cannot be exactly identical, since their corresponding diffraction patterns are different). This suggests that the vacancy clustering that exists in low bornite also exists in  $2a-I$ . This conclusion is inconsistent with the twinning model which had been used to explain the extinctions.

It is appropriate to consider alternate models to that proposed by Morimoto (1964) for the  $2a-I$  struc-

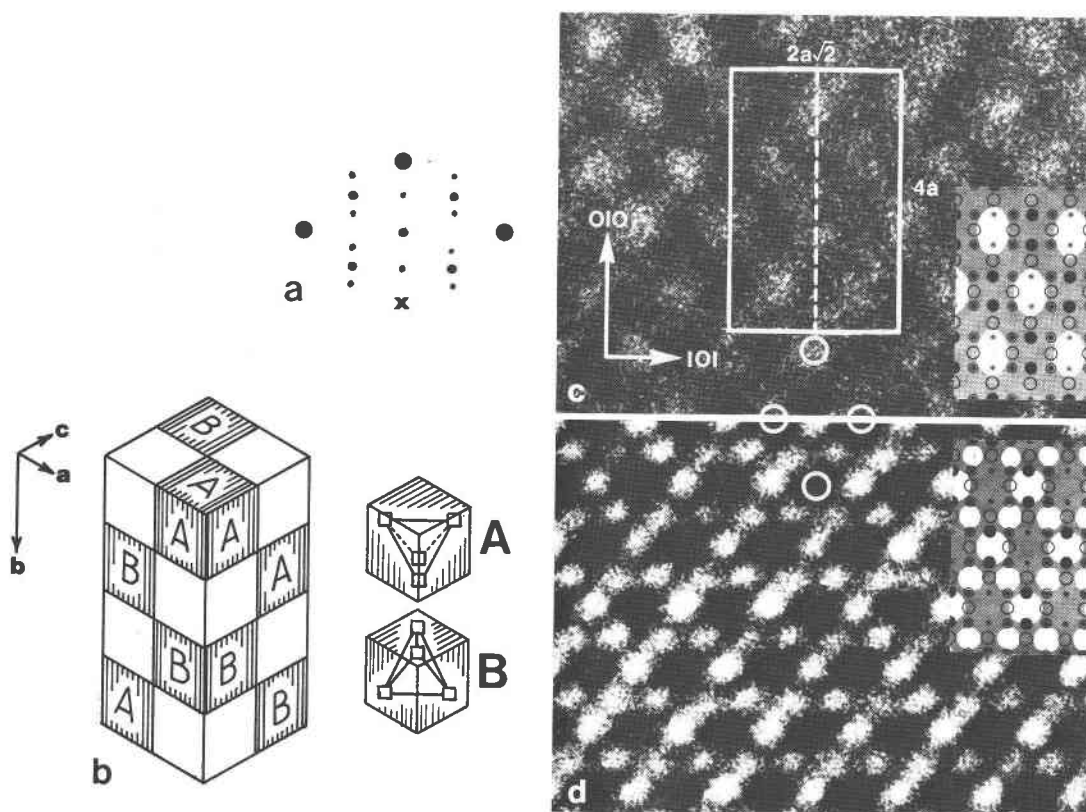


Fig. 5. Low bornite ( $2a4a2a$ ) (Magma, Arizona). (a) The diffraction pattern of low bornite. (b) The low bornite structure (after Koto and Morimoto, 1975). White cubes represent subcells with all metal sites filled. Hatched cubes represent subcells with four vacancies and four filled sites. The vacancies (small squares in the right-hand drawings) can occur in one of two orientations, marked *A* and *B*. Thus, superstructuring in low bornite consists of an alternation of vacancy-rich and vacancy-poor regions within the unit cell, producing a compositional modulation in three dimensions. Electron structure images indicate that similar modulations in composition occur throughout the bn-dg series, and are an essential component of superstructuring. (c) A bright-field image of low bornite. A projected unit cell is drawn onto the image. The schematic inset shows the relationship between the projected structure and the contrast observed in the image, as determined by computer simulation. In the projected structure, metal sites have a relative occupancy of either 1.0 (large solid circles), 0.75 (large double circles) or 0.50 (small double circles); sulfurs are represented by open circles. The white areas in the image are centered about the positions of 0.5 metal occupancy, and thus represent the positions of the vacancy-rich clusters in the structure. Several of these clusters are marked by white circles on the image. (d) A dark-field image. In this case, regions of high vacancy concentration are represented by large black areas in the image. Thus, contrast in the dark-field image is approximately the reverse of the bright-field image. To illustrate this, the photographs have been mounted so that the structure is continuous. Additionally, regions of high vacancy concentration have been highlighted by white circles, as in (c). The schematic inset shows the image to structure relationship similarly to the inset in (c). Images of the  $2a-I$  and  $2a-II$  structures appear identical to this image of low bornite.

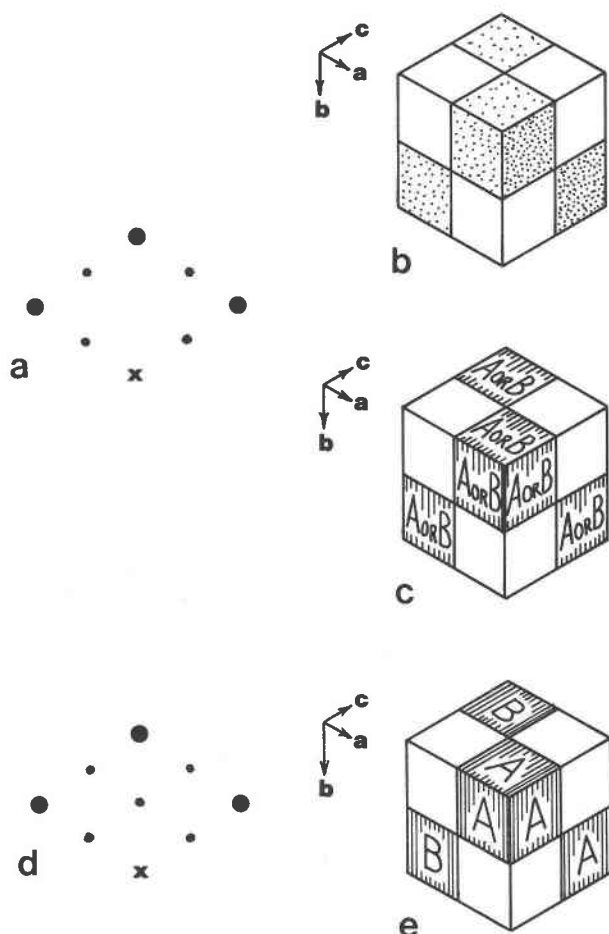


Fig. 6. The  $2a$  superstructures (Magma, Arizona bornite starting material). (a) The diffraction pattern of  $2a-I$ . (b) Hypothetical structure model 1 for the  $2a-I$  structure. White cubes represent subcells containing filled metal sites. Stippled cubes represent subcells containing a disordered array of metal atoms and vacancies producing an average metal-site occupancy of 0.5. (c) Hypothetical structure model 2 for the  $2a-I$  structure. Hatched cubes represent ordered arrangements as for low bornite, but in this case there is an equal probability of a given subcell being in either A or B orientation. (d) The diffraction pattern of the  $2a-II$  structure. (e) A hypothetical structure model for the  $2a-II$  structure, with the same notation as in Fig. 5b. This model is similar to the low bornite structure, but without the change of orientation of the vacancy-containing subcells in the  $b$ -direction.

ture. This structure changes gradually into low bornite over a period of a week at room temperature (Morimoto and Kullerud, 1961), so it might be expected that  $2a-I$  is a disordered modification of the low bornite structure. More importantly, disorder can produce the proper extinctions and superstructure in two ways while maintaining the vacancy cluster framework. Within each cluster either: (1) vacancies are disordered among the eight sites (Fig. 6b), or (2) vacancies are ordered as in low bornite,

but, rather than having a definite arrangement of cluster orientations (as in low bornite), the orientation of each cluster has an equal probability of being either A or B (Fig. 6c).

These two possibilities cannot be distinguished, either in image or diffraction pattern, without refinement. Of the two, however, the latter is more likely, since short-range ordering of vacancies is maintained. Although these models reproduce the extinctions of the  $2a-I$  structure, their calculated X-ray intensities (assuming ideal metal and sulfur positions) do not closely match the experimental intensities given by Morimoto (1964). A new refinement of the  $2a-I$  structure is indicated.

#### $2a-II$

This structure was not reported by Morimoto and Kullerud (1961) in their study of bornite polymorphs. However, a  $2a-II$  electron diffraction pattern (Fig. 6d) was reported by Putnis and Grace (1976). Multiple electron diffraction is capable of producing significant intensity in the normally-extinct  $\{002\}_{\text{super}}_{\text{cell}}$  reflections of  $2a-I$ , giving the appearance of a  $2a-II$  structure, but their observations of transformations between the two phases (confirmed in this study) leave no doubt that a  $2a-II$  structure does exist. It can be produced in the microscope during both slow heating of low bornite and cooling of material having the  $2a-I$  structure. Images of  $2a-II$  appear the same as images of  $2a-I$  and low bornite. Diffraction patterns of  $2a-II$  have a full complement of superstructure reflections, so the disorder hypothesized for  $2a-I$  need not be present in  $2a-II$ . A likely explanation is that the structure of  $2a-II$  is ordered similarly to low bornite, but does not have the reversal of vacancy-cluster orientation in the  $b$ -direction that low bornite has (Fig. 6c).

A continuous gradation between the  $2a-I$  and  $2a-II$  types can be observed in electron diffraction patterns. This is presumably due to a continuous ordering process. Thus, for the bornite composition, we have seen a number of gradual superstructuring stages which take place upon cooling of the  $1a-I$  structure: (1) incipient vacancy clustering, (2)  $2a-I$ , (3)  $2a-II$ , and (4) low bornite. Each of these stages is closely related to the others by the existence of vacancy clusters, and each succeeding stage apparently represents a slightly more ordered modification of the last.

#### Digenite, $5a-I$ , $Na-I$

Donnay *et al.* (1958) reported natural digenite with a  $5a-I$  diffraction pattern (Fig. 7a). However, Mori-

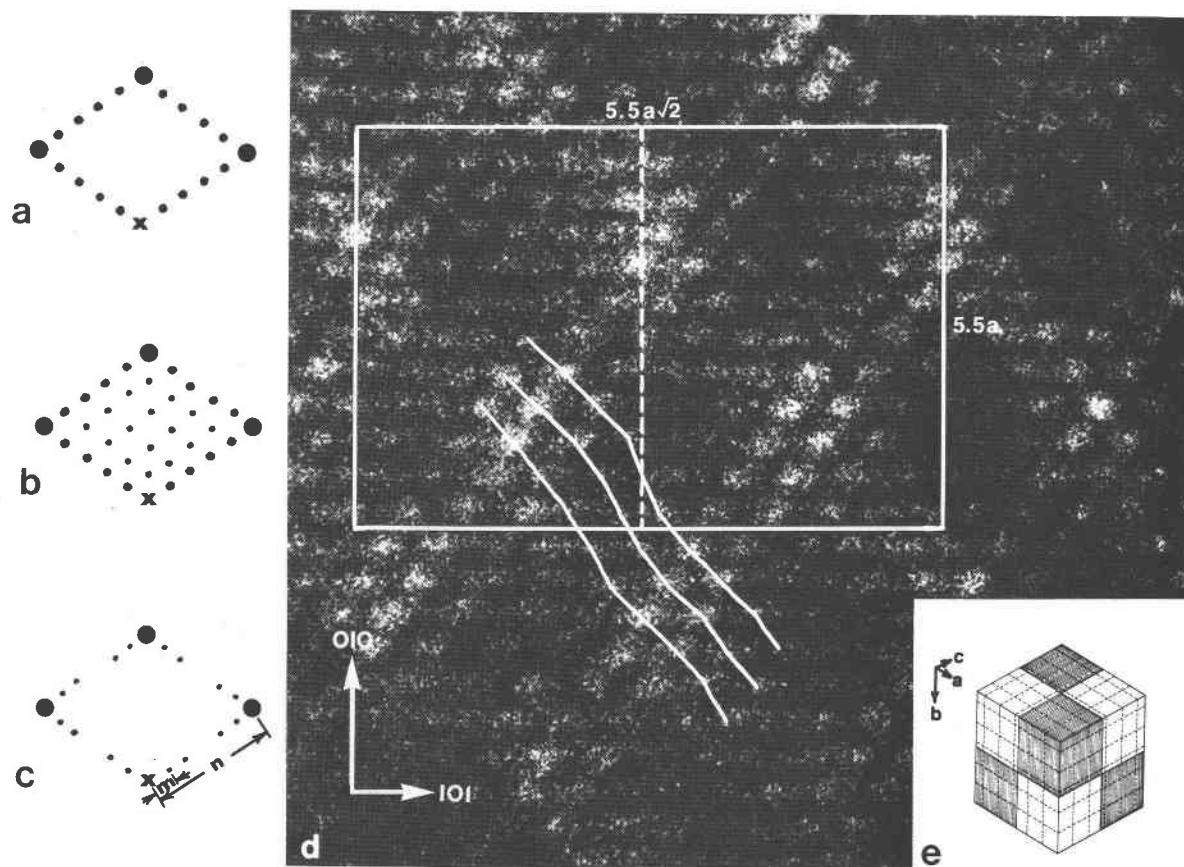


Fig. 7. Digenite superstructures (Butte, Montana). (a) The diffraction pattern of the  $5a-I$  structure. (b) The diffraction pattern of  $5a-II$ . (c) The diffraction pattern of  $Na-I$ .  $N$  is determined by dividing  $n$  by  $m$ . (d) A dark-field image of the  $Na-I$  structure, with  $N = 5.5$  as determined from the diffraction pattern. The unit cell is drawn onto the image. The pattern of dot intensities is similar to that in images of low bornite, but on a larger scale. The image can be explained by a model containing alternating regions of vacancy-rich and filled sites, similar to the structure of low bornite. This model is illustrated in (e). The contrast in the image could be described as well by a sinusoidal modulation of metal-site occupancy throughout the crystal (not illustrated). There is displacement of the dots in the image from their idealized (colinear along  $(111)$ ) positions, as shown by the white lines drawn through the dots. This distortion is presumably a response to the compositional modulation in the structure. The distortion appears more prominent in certain directions than others which should be crystallographically identical, probably due to a slight tilt of the crystal. (e) A hypothetical, idealized model of the  $Na-I$  structure. A unit cell of dimensions  $5.5a$  has been divided into octants, four of which contain filled metal sites (white cubes) and four of which contain filled and vacant sites (hatched cubes.)

moto and Kullerud (1963) reported  $5a-I$  as metastable, and  $5a-II$ ,  $Fm\bar{3}m$ , (Fig. 7b) as stable. Additionally, non-integral ( $Na$ ) superstructures can occur in natural digenites (Morimoto and Gyobu, 1971).

With the electron microscope,  $5a-I$  and  $Na-I$  structures of digenite were observed.  $5a-II$  was not observed. In  $Na-I$  the spacings of the superstructure spots are not positioned at exactly integral multiples of one-fifth the spacing of the subcell spots. Instead, the spacings are indicative of a supercell slightly larger than  $5a$  (Fig. 7c). The occurrence of the  $Na-I$  superstructure in digenite is either because of transformation from the  $5a$  types by electron bombardment, or because the sample initially contained  $Na-I$ .

Figure 7d shows a dark-field image of an  $Na-I$  structure,  $N = 5.5$ , determined from the electron diffraction pattern. Areas containing the dimmest dots in the image probably represent positions of clusters of vacancy-rich sites in the superstructure. The vacancy clusters have dimensions approximately half those of the supercell (Fig. 7e). Intensity fluctuations in the image are consistent with either roughly equidimensional clusters of relatively homogeneous vacancy concentrations (over the vertical projection of  $\sim 5$  unit cells during imaging), or sinusoidal modulations in metal site occupation and position with periodicity  $= N$ . The image is similar to that of  $2a-I$ , except for the larger scale of the superstructure. Thus,

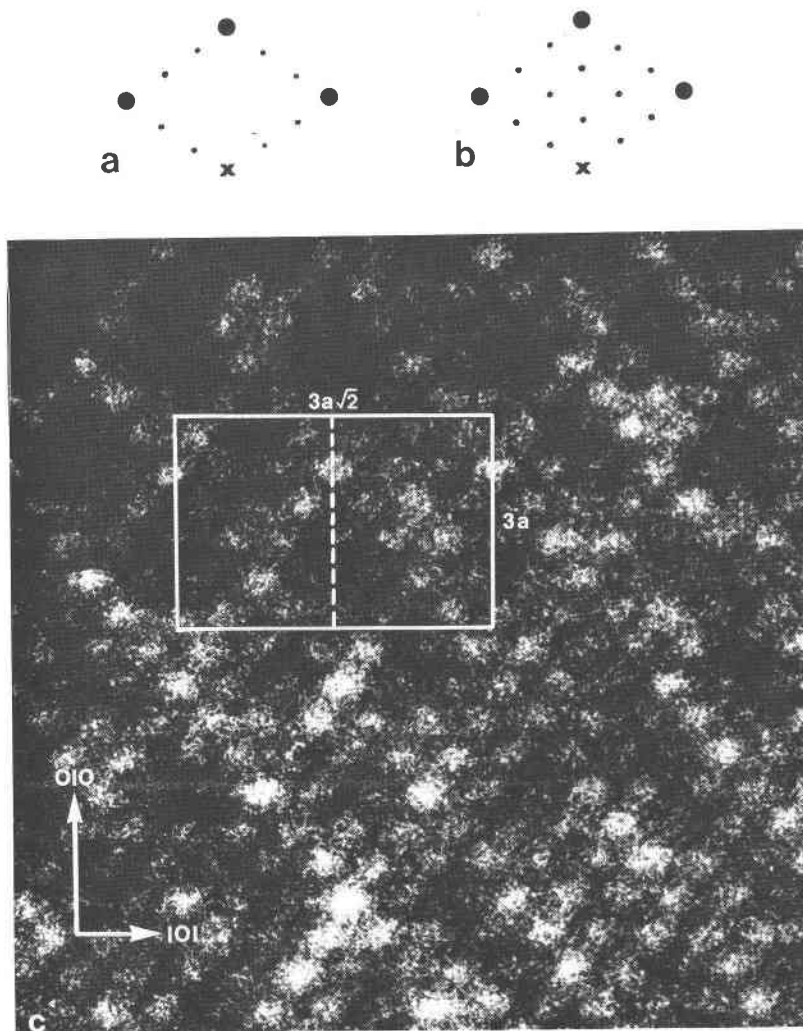


Fig. 8. The  $3a$  superstructures (Magma, Arizona bornite starting material). (a) The diffraction pattern of the  $3a-I$  structure. (b) The diffraction pattern of the  $3a-II$  structure. (c) A dark-field micrograph of the  $3a-I$  structure ( $3a-II$  appears identical). The intensity variations in the image, although on a different scale, are similar to those in images of low bornite and digenite, indicating a structure similar to the previously discussed models.

the  $2a-I$  and  $Na-I$  structures appear to share a common superstructuring mechanism involving vacancy clustering.

It was possible to hypothesize two models for the  $2a-I$  superstructure that reproduce the extinctions and superstructure spots seen in its diffraction pattern. A model for the  $5a-I$  structure was formulated similarly to those for the  $2a-I$  structure, except with the larger disordered vacancy clusters indicated by the images. It was found, however, upon calculation of diffracted intensities for the model, that only the  $111_{\text{supercell}}$  or  $1/5\ 1/5\ 1/5_{\text{supercell}}$  reflection was reproduced along with the required extinctions. The  $222$ ,  $333$ , and  $444_{\text{supercell}}$  reflections present in  $5a-I$  diffrac-

tion patterns were not reproduced by the model. Additional features, such as distortion (discussed below), need to be included to obtain a satisfactory match between calculated and observed diffraction patterns.

#### $3a-I$ , $3a-II$ , $4a-I$ , $4a-II$ , $6a-I$

These members of the bn-dg series were produced in the microscope by heating with the electron beam, as discussed in the Experimental section. Figures 8, 9, and 10 show diffraction patterns and images of superstructures of  $3a$ ,  $4a$ , and approximately  $6a$  periodicity, respectively. Figure 10b consists of a mixture of  $5a$  and  $6a$  periodicities. This indicates that the

vacancy clusters have varied size and spacings. Since a non-integral  $Na$ -type superstructure is known to occur, such a mixture of  $5a$  and  $6a$  periodicities is reasonable. For this reason, and because of the great distortion shown in the image of the  $6a$ -I structure, the concept of a unit cell is inappropriate and so the unit cell is not drawn in the image.

The images of superstructures of  $3a$ ,  $4a$ , and  $6a$  periodicity share the features of the previously-discussed  $2a$ ,  $5a$  and  $Na$  superstructures. That is: the superstructures, whether *type I* or *type II*, share vacancy clustering as an essential part of superstructuring, and thus images of the *type I* and *type II* structures having the same supercell dimensions appear identical in electron microscope images. Where

both *type I* and *type II* have been observed, there seems to be a continuous transformation between them during beam-heating experiments. Vacancy-containing clusters seem to be equidimensional in shape upon imaging, as well as appearing to contain fairly homogeneous concentrations of vacancies.

#### Other superstructures

*1a1a2a-1*. Figure 11a shows a superstructure that was formed in the microscope during approximately 30 minutes heating of a bornite crystal at temperatures below the  $1a$ -I transition. The smallest unit cell consistent with the spacings in the image has dimensions  $1a1a2a$ . The domain grew slowly for 10 minutes, could not be reproduced once the crystal

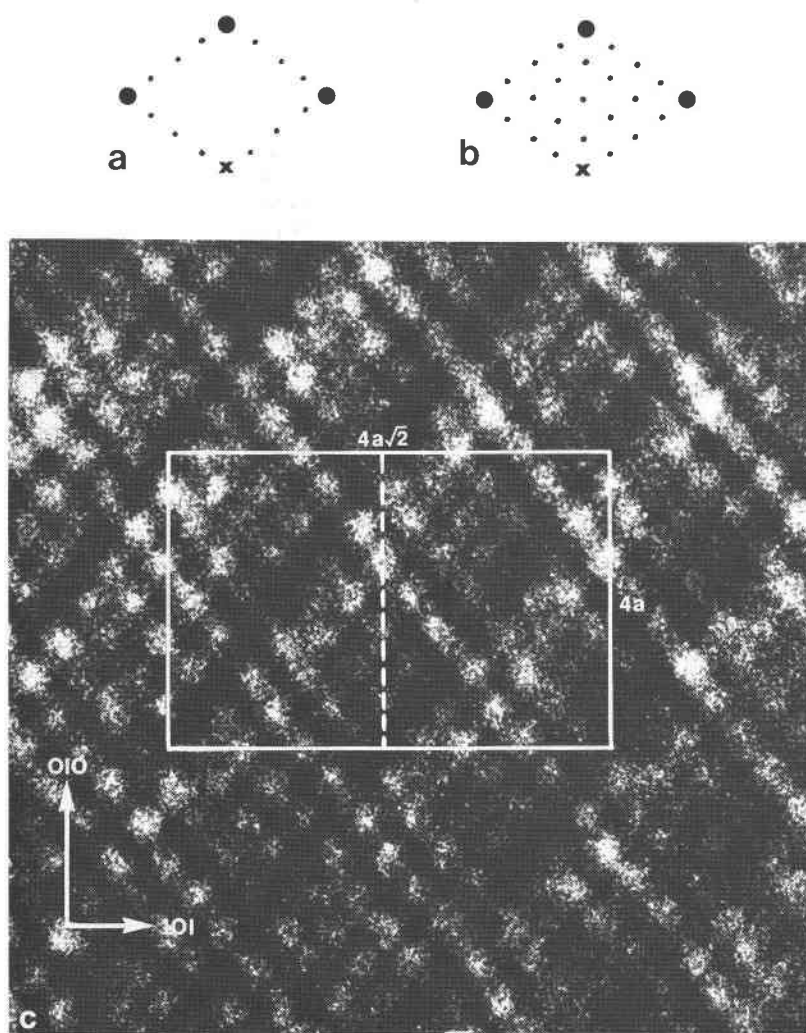


Fig. 9. The  $4a$  superstructures (Magma, Arizona, bornite starting material). (a) The diffraction pattern of the  $4a$ -I structure. (b) The diffraction pattern of the  $4a$ -II structure. (c) A dark-field image of a superstructure of  $4a$  periodicity, showing features in common with images of other members of the  $bn$ - $dg$  series.

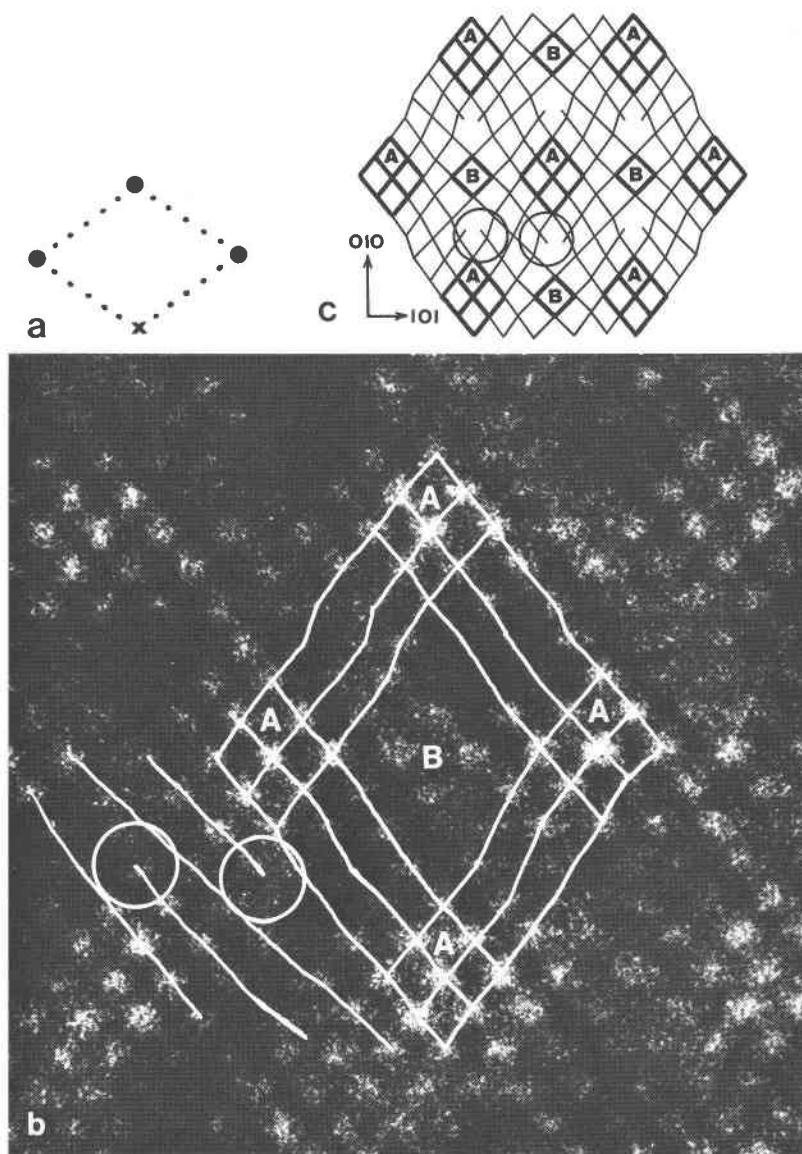


Fig. 10. The  $6a-1$  structure (Butte, Montana, digenite starting material). (a) A portion of the diffraction pattern of  $6a-1$ . (b) A dark-field image from a crystal having the above diffraction pattern. Vacancy clusters vary in size throughout the image (see text), and distortion is marked (accentuated by drawn lines). Areas labelled *A* and *B* in the image correspond to periodically-alternating regions of different structure in the crystal. Thus, the  $6a-1$  structure (and the entire series of bn-dg superstructures which show similar distortion) may result from spinodal decomposition (see text for full discussion). Discontinuous rows of dots (circled) seem to be the result of the mismatch of the lattice spacings of the two structures. (c) An idealized representation of (b), showing only the lines.

was heated to the  $1a-1$  structure, and was not observed in other crystals. For these reasons, it is thought to be metastable, an example from what is possibly a large number of ordered or semi-ordered phases that can occur metastably in the bn-dg series.

*1a1a2a-2*. Another superstructure is shown in Figure 11b. The image is of particular significance for consideration of the usefulness of dark field imaging. It consists of rows of dots 1.9A apart, giving an

apparent point-to-point resolution of less than  $2A$ . Thus, on a given microscope, dark-field imaging is capable of giving detail at almost half the scale observable with bright-field. Again, the smallest unit cell consistent with the spacings in the diffraction pattern of the structure (Fig. 11c) has dimensions  $1a1a2a$ , here called  $1a1a2a-2$ . The  $1a1a2a-2$  structure was observed many times in beam-heating experiments with bornite. It was sometimes observed during quenching

from  $1a-1$ , and sometimes after heating the  $2a$  types at temperatures below the  $1a-1$  transition. All transformations to this structure are abrupt, involving almost instantaneous changes of hundreds or thousands of unit cells.

#### Anti-phase domains

Putnis and Grace (1976) hypothesized that the non-systematic extinctions in the  $2a-1$  structure are caused by the existence of anti-phase domains. We have, on occasion, seen anti-phase domains in images of bornite (Fig. 12). The simplest explanation of the observed images involves an offset in vacancy distribution. The displacement,  $[(a+b)/2]_{\text{subcell}}$  is projected along  $\langle 111 \rangle$  in the image. From the width and direction of the projections of the anti-phase boundaries, the plane of the boundaries appears to approximately parallel a  $\{111\}$  plane. Contrary to Putnis and Grace, we do not believe that these anti-phase domains produce the non-systematic extinctions in the  $2a-1$  struc-

ture, because anti-phase domains are not often seen in images of  $2a-1$ , and show little tendency to coarsen to produce  $2a-11$ .

#### Structural distortion and superstructuring

In the image of the  $1a-1$  structure (Fig. 4b), dots are colinear along  $\langle 111 \rangle$ . However, the superstructure images show displacement of the dots from linearity.<sup>1</sup> Furthermore, displacement increases with the superstructure size. The distortion is shown by drafted lines in Figures 7d and 10b. In the  $6a-1$  structure, the distortion is so great that periodically-alternating regions of two distinct structures can be identified, marked A and B in Figure 10b (not to be confused with the vacancy orientations of Fig. 5). In regions A,

<sup>1</sup> From the standpoint of electron microscopy, it is interesting that this distortion would not be seen in the conventional bright-field mode. The dots representing the subcell structure and showing the distortion are only seen using high-resolution dark-field techniques.

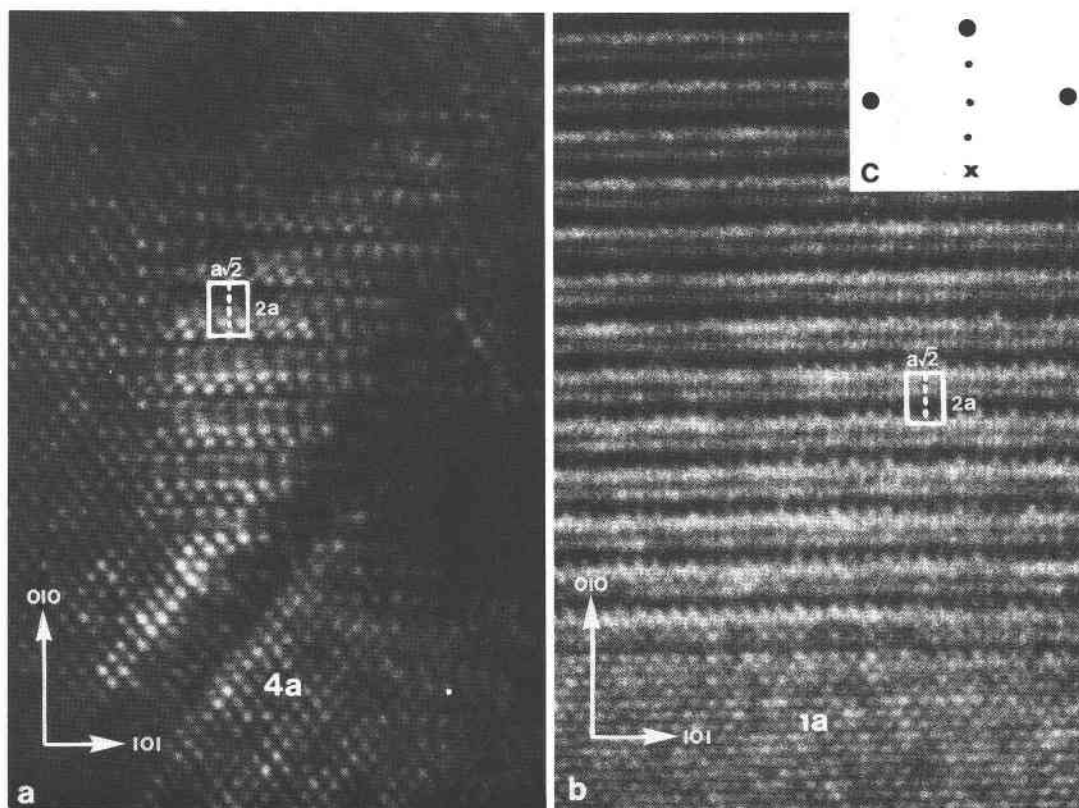


Fig. 11. The  $1a1a2a$  superstructures (Magma, Arizona, bornite starting material). (a) A dark-field image of the  $1a1a2a-1$  structure, with a unit cell indicated. The small region of this structure appears next to a faulted zone (heavy black band) and is surrounded by a structure of  $4a$  periodicity. (b) A dark-field image of  $1a1a2a-2$ . The lower part of the photograph contains the  $1a-1$  image, showing that imaging conditions were the same for this micrograph as for others in this paper. The  $1a1a2a-2$  image consists of rows of dots  $1.9\text{\AA}$  apart in the  $[101]$  direction, showing detail on half the scale theoretically possible using bright-field mode under the same instrumental conditions. This illustrates the great potential of dark-field imaging in structure analysis. (c) The diffraction pattern of the  $1a1a2a-2$  structure.

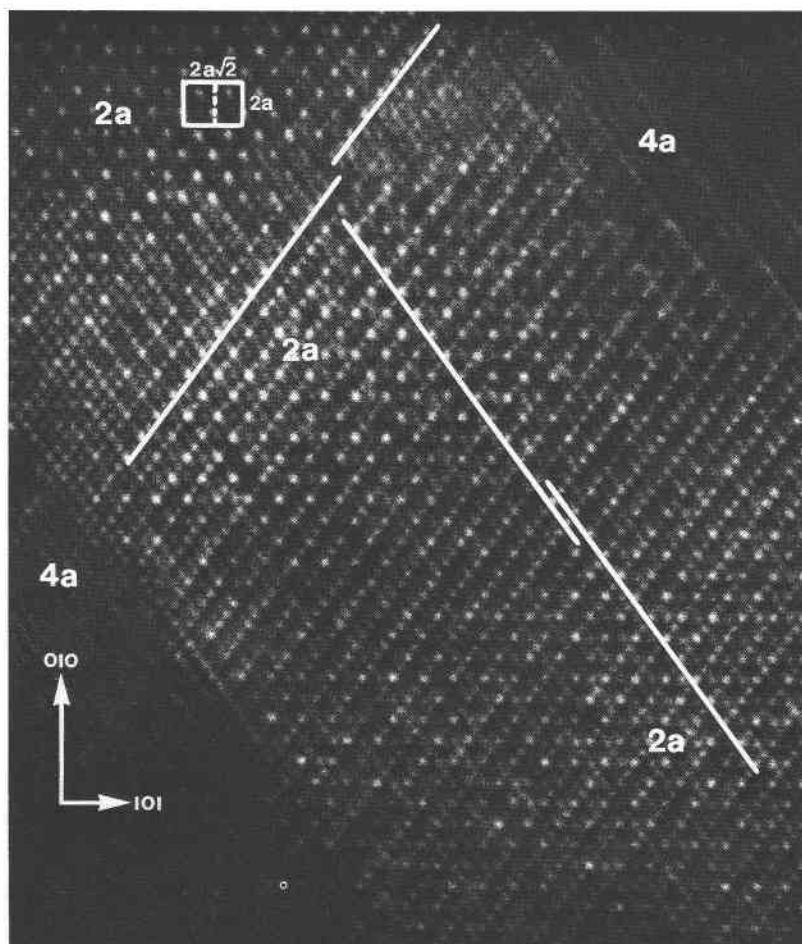


Fig. 12. Antiphase domains in Magma, Arizona, bornite. In this sample which had been heated in the electron beam, three domains of  $2a$  periodicity appear within a domain of  $4a$  periodicity. The white lines are drawn directly beneath rows of bright dots to highlight the anti-phase relationships between the  $2a$  domains. The top antiphase boundary has an offset in the *NW* direction while the bottom antiphase boundary has an offset in the *NE* direction.

angles between rows of dots average  $75^\circ$ , while in regions B angles are commonly near  $90^\circ$ . Rows of dots appear to terminate (circled), resulting from the mismatch of superlattice spacings. An idealized representation of the structure in Figure 10b is given in Figure 10c.

The  $6a-1$  structure seems to represent an unmixing of two structures. Additionally, there is a periodic compositional modulation in the low bornite structure as determined by X-ray analysis (Koto and Morimoto, 1975). Similarities in the positions and intensities of dots in electron images of the bn-dg structures indicate a similar superstructuring mechanism for the entire series. It therefore seems that superstructures in the series arise from periodic structural and compositional modulations. These modulations are highly suggestive of the first stages of

exsolution of vacancy-rich and vacancy-poor regions, and a spinodal mechanism is a possibility. The vacancy-poor regions, which in low bornite approximate chalcocite in composition (Koto and Morimoto, 1975), might be expected to also approximate chalcocite in structure, especially in the larger superstructures that apparently contain large volumes of this composition. Indeed, Figure 10b contains areas (B) in which the contrast is similar to what we would predict from metal atoms tetrahedrally-coordinated to hexagonally closest-packed sulfurs (the chalcocite structure). Therefore, in observing the bn-dg series, we may have the chance to watch the first stages of the unmixing of a hexagonal from a cubic closest-packed species. If our samples are representative, then the bn-dg superstructures, seemingly being arrested in the process of exsolution, are thus meta-

stable, despite their widespread occurrence in nature. The anomalous bornites with compositions more metal-deficient than bornite (Brett and Yund, 1964) may also be a result of similar arrested exsolution.

### Summary

Both bright- and dark-field high-resolution electron microscopy are well suited for the study of complex structures in sulfides. In the bn-dg series we have found that dark-field imaging gives greater contrast and resolution than bright-field, and provides detail at the sub-unit-cell level. Complete interpretation of dark-field micrographs is difficult, owing to the lack of adequate computer-simulation techniques. However, in cases such as the bn-dg series, in which the subcell structure and the low bornite structure are well known, a relationship between image and structure can be established and then applied to related but unknown structures.

Superstructuring in the series takes place through a number of stages: (1) incipient vacancy clustering, producing diffraction patterns with diffuse satellite peaks, (2) the formation of the *type I* superstructures, producing diffraction patterns that contain numerous non-systematic extinctions, (3) the formation of the *type II* superstructures, producing diffraction patterns with a full complement of superstructure reflections, (4) the formation of non-cubic superstructures of larger dimension than the *type II* structures (such as low bornite). Transformation between the stages appears, in many cases, to be continuous over a range of temperatures.

Electron imaging indicates that the superstructuring process in the bn-dg series involves the formation of vacancy-rich and vacancy-poor regions, which alternate in a three-dimensional checkerboard fashion. This alternation gives rise to a modulation of composition and of atomic positions. Additionally, alternating regions of differing structure are present in the  $\delta a-I$  structure, and similar distortion can be seen in the remaining members of the series. These features imply an unmixing of composition and structure in the bn-dg series. The various stages in superstructuring observed upon cooling these compounds may be interpreted in terms of unmixing. The diffuse reflections in diffraction patterns, corresponding to the initial superstructuring upon cooling, arise from the unmixing of vacancy-rich and vacancy-poor regions, the vacancies being still disordered on a sub-unit-cell level. The stages that follow then represent successive short-range ordering schemes of the vacancies within the framework of the compositional

modulation. The ordering of vacancies may itself contribute heavily to the arresting of the unmixing process by lowering the free energy of the crystal below that required to overcome the activation energy of continued exsolution.

It thus appears that superstructures in the bn-dg series arise from a combination of compositional and structural modulations and short-range vacancy ordering. If this is due to arrested exolutions, bornite and digenite are not phases in the classical sense, but are metastable "mixtures" of structures. However, bornite and digenite exhibit equilibrium-like relationships with other minerals, as determined by many synthesis experiments (e.g. Craig, 1974). The chemical interactions giving rise to a complex sequence of superstructures such as the bn-dg series are not understood at present, and may be a fruitful area for further investigation. Also, the relationships of bornite and digenite structures to their associates in nature, as well as to prevailing geologic conditions, are yet to be determined. Implications from the nature of superstructuring in the bn-dg series are far-reaching, and impinge upon many other compounds having superstructures. In the investigation of these implications, it is certain that high-resolution electron microscopy, and particularly the contribution of high-resolution dark-field electron microscopy, will be significant.

### Acknowledgments

We thank Drs. J. M. Cowley and R. Von Dreele for stimulating comments and discussion during this study and Drs. C. T. Prewitt and R. A. Yund for helpful reviews. We also thank John Wheatley for his help throughout the study. Experimental work was done using the high-resolution electron microscope facility of the Center for Solid State Studies at Arizona State University. Financial support was provided by NSF grants DES74-22156 and EAR77-00128.

### References

- Brett, R. and R. A. Yund (1964) Sulfur-rich bornites. *Am. Mineral.*, 49, 1084-1098.
- Buseck, P. R. and S. Iijima (1974) High resolution electron microscopy of silicates. *Am. Mineral.*, 59, 1-21.
- Cowley, J. M. (1975) *Diffraction Physics*. North-Holland Publishing Company, Amsterdam.
- and S. Iijima (1976) The direct imaging of crystal structures. In H. R. Wenk, Ed., *Electron Microscopy in Mineralogy*, p. 123-136. Springer-Verlag, Heidelberg.
- Craig, J. R. (1974) The Cu-Fe-S system. *Sulfide Mineralogy, Mineral. Soc. Am. Short Course Notes*, Vol. 1, CS64-CS76.
- Donnay, G., J. D. H. Donnay and G. Kullerud (1958) Crystal and twin structure of digenite. *Am. Mineral.*, 43, 228-242.
- Fruh, Jr., A. J. (1950) Disorder in the mineral bornite,  $\text{Cu}_5\text{FeS}_4$ . *Am. Mineral.*, 35, 185-192.
- Iijima, S. (1973) Direct observation of lattice defects in  $\text{H-Nb}_2\text{O}_6$ .

- by high resolution electron microscopy. *Acta Crystallogr.*, *A29*, 18-24.
- Koto, K. and N. Morimoto (1970) The crystal structure of anilite. *Acta Crystallogr.*, *B26*, 915-924.
- and —— (1975) Superstructure investigation of bornite,  $\text{Cu}_5\text{FeS}_4$ , by the modified partial Patterson function. *Acta Crystallogr.*, *B31*, 2268-2273.
- Manolikas, C., P. Delavignette and S. Amelinckx (1976) Electron microscopy of phases in the  $\text{Cu}_{2-x}\text{S}$  system, *Phys. Status Solidi*, *a33*, K77-K79.
- Morimoto, N. (1964) Structures of two polymorphic forms of  $\text{Cu}_5\text{FeS}_4$ . *Acta Crystallogr.*, *17*, 351-360.
- and A. Gyobu (1971) The composition and stability of digenite. *Am. Mineral.*, *56*, 1889-1909.
- and G. Kullerud (1961) Polymorphism in bornite. *Am. Mineral.*, *46*, 1270-1282.
- and —— (1963) Polymorphism in digenite. *Am. Mineral.*, *48*, 110-123.
- and —— (1966) Polymorphism on the  $\text{Cu}_5\text{FeS}_4$ - $\text{Cu}_9\text{S}_5$  join. *Z. Kristallogr.*, *123*, 235-254.
- Pierce, L. and P. R. Buseck (1974) Electron imaging of pyrrhotite superstructures. *Science*, *186*, 1209-1212.
- and —— (1975) High resolution electron microscopy of sulfides (abstr.). *Geol. Soc. Am. Abstr. with Programs*, *7*, 1229.
- and —— (1976) A comparison of bright field and dark field imaging of pyrrhotite structures. In H. R. Wenk, Ed., *Electron Microscopy in Mineralogy*, p. 137-141. Springer-Verlag, Heidelberg.
- Putnis, A. (1977) Electron diffraction study of phase transformations in copper sulfides. *Am. Mineral.*, *62*, 107-114.
- and J. Grace (1976) The transformation behavior of bornite. *Contrib. Mineral. Petrol.*, *55*, 311-315.
- Skarnulis, J. (1975) *A Computer Program System for the Study of Materials Using n-Beam Dynamical Image Calculations*. PhD Thesis, Arizona State University.
- Tunell, G. and C. E. Adams (1949) On the symmetry and crystal structure of bornite. *Am. Mineral.*, *34*, 824-829.

*Manuscript received, April 13, 1977; accepted  
for publication, July 18, 1977.*